Subwavelength optical imaging through a silver nanorod

Yuan-Fong Chau
Ching Yun University
Department of Electronic Engineering
Jung Li, Taiwan
E-mail: yfc01@cyu.edu.tw

Din Ping Tsai, FELLOW SPIE
National Taiwan University
Department of Physics and Center for Nanostorage Research
Taipei, Taiwan

Guang-Wei Hu
Chinese Army Academy
Department of Electrical Engineering
Kaohsiung, Taiwan

Lin-Fang Shen
Electromagnetic Academy
Department of Information Science and Electronic Engineering
Zhejiang Province
Hang Zhou 310027, China

Tzong-Jer Yang
National Chiao-Tung University
Department of Electrophysics
HsinChu 300, Taiwan

Abstract. We numerically investigated subwavelength imaging in a silver nanorod of 50-nm height and 20-nm diam buried in dielectric background (SiO_2) with a finite-difference time-domain (FDTD) method in the three dimensions. The near-field components of the Gaussian incident beam were plasmonically transferred through the input end of a silver nanorod to reproduce the light distributions of the incident wave at the output end. The field distributions were calculated at the different sectional planes of the rods, and it was found that the spatial resolution was less than 40 nm given by the rod size, which is much beyond the diffraction limit of the conventional imaging system. The field intensity in the image plane was well resolved due to the collection of surface plasmon polaritons. The behaviors of the three components of field distribution at entrance and exit from the nanorod and the influences of the optical field distribution generated by some factors are also discussed in detail. The proposed structure possesses a deep transfer of super-resolution image and can be used with image transfer. © *2007 Society of Photo-Optical Instrumentation Engineers.*
[DOI: 10.1117/1.2715929]

Subject terms: subwavelength imaging; finite-difference time-domain (FDTD) method; surface plasmon polaritons; image transfer.

Paper 060343CR received May 10, 2006; revised manuscript received Sep. 21, 2006; accepted for publication Sep. 26, 2006; published online Mar. 29, 2007.

Due to conduction, electron charge density and its corresponding electromagnetic field can undergo plasmon oscillations, and metallic materials on a nanoscale can be used to enhance and exploit properties that become stronger under conditions of reduced dimensionality. The optical properties of metallic nanoparticles that the charge oscillations can propagate along the surface at optical frequencies and their mechanism to concentrate light into highly confined regions has attracted considerable interest for a broad range of applications.[1–3] The use of a sharpened metallic tip as a probe in near-field scanning optical microscopy (NSOM) is proposed.[4–6] This configuration has been applied to nano-imaging and analysis, including infrared absorption,[7] spontaneous Raman scattering,[8] and coherent anti-Stokes Raman scattering.[9] A concentric metallic nanoshell showed strong coupling with resonant surface plasmons at the near-infrared (IR) spectra, and this technology was applied to biological sensors and labels.[10] Periodically arranged nano-slits or nano-holes were investigated in metal film beam anomalous light as a collection of surface plasmon polaritons (SPPs).[11–13] Recently, subwavelength image transfer, which is another interesting property of metallic nanostructures,[14–16] was proposed by Ono et al.[17] in a subwavelength imaging transfer system that set the nanoarray in air background and used a point source as the incident light focused onto the input end of the array. Although some significant optical properties were found in the near-field zone, this system is hard to follow, and some drawbacks in realizing this super-resolution in image transfer systems are found, because the nanoarray must be buried in dielectric materials such as glass, polymer, or alumina, and the simulated incident wave must be a Gaussian wave (to imitate the laser beam) in order to simulate a real-word situation.

Motivated by the previous work cited here and inspired by these active issues, in this study, we investigated subwavelength imaging of a silver nanorod by using the three-dimensional (3D) finite-difference time-domain (FDTD) method.[18] The influences of the optical field distribution generated by some factors in a silver (Ag) nanorod will be discussed in detail.

The structure we studied here is an Ag nanorod. Figure 1 shows the side view of a single Ag nanorod with diameter $d=20$ nm and height $h=50$ nm buried in dielectric material (SiO_2, refractive index $n=1.5$). The rod diameter is much less than the wavelength, and the rod axis is parallel to z axis. In our numerical simulation, the 3D FDTD method with perfectly matched layer boundary conditions[19] is used to analyze the mechanism of plasmonic image transform. The dispersive behavior of the Ag nanorod is simulated by the Lorentz model.[20] This analysis reveals several intriguing features of light propagation in the Ag nanorod. In particular subwavelength resolution can be achieved with the Ag nanorod when the localization of the light wave is

0091-3286/2007/$25.00 © 2007 SPIE

Downloaded From: http://opticalengineering.spiedigitallibrary.org/ on 04/26/2014 Terms of Use: http://spiedl.org/terms

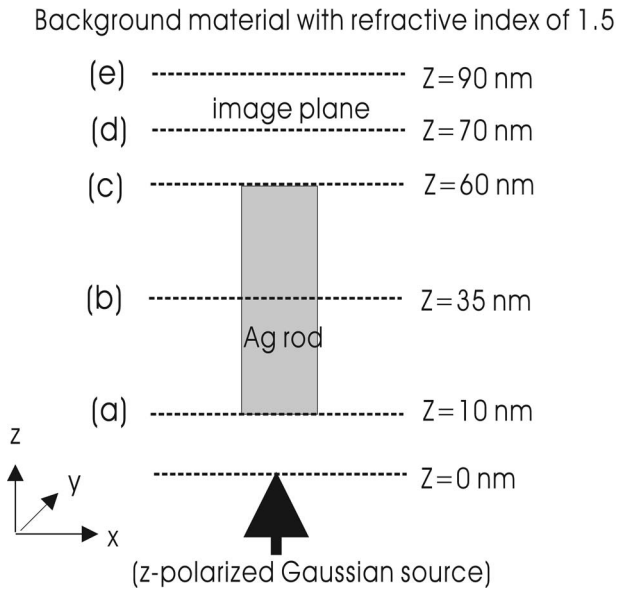

Fig. 1 Side view of a silver nanorod with a diameter of 20 nm and a height of 50 nm.

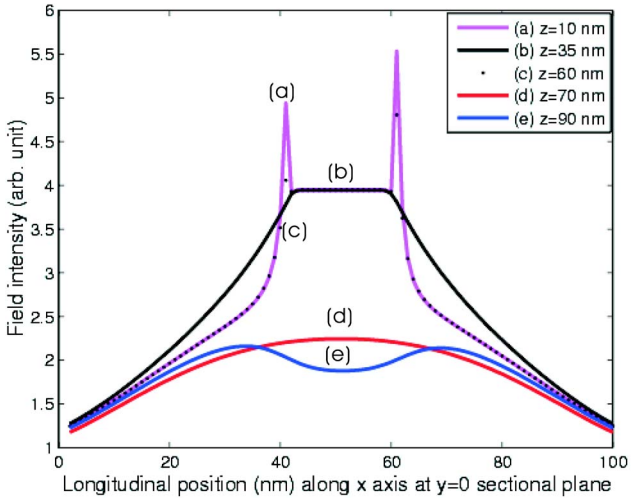

Fig. 2 The field intensity along x (at $y=50\ \delta$ sectional plane shown in Fig. 1) in the plane of (a) $z=10$ (the bottom of the rod), (b) $z=35$ (the center of the rod), (c) $z=60$ (the top of the rod), (d) $z=70$ (imaging plane), and (e) $z=90$ (at 30-nm plane away from the top of rod).

within areas whose sizes are less than a wavelength. This provides the information concerning the spatial distribution of the electromagnetic field emerging from the output end of the Ag nanorod.

First, we observed the field distribution with the 3D FDTD method of an Ag nanorod. The z-polarized input Gaussian beam with wavelength of 488 nm (to have a resonance of plasmon oscillation of Ar^+ laser excitation at wavelength of 488 nm) and implemented as an SF/TF (scattering field/total field) source[21] is focused onto the central part of the Ag nanorod, located at the center of the rod bottom. The nanorod is located 10 nm away from the incident beam at normal angle, as shown in Fig. 1. In order to implement this optical image transfer system as an optical device, the Ag nanorod must be buried in a dielectric background. We chose SiO_2 as a dielectric medium, which has a refractive index of 1.5. The SiO_2 is used to imitate a silica waveguide (SWG), as shown in Fig. 1. An Ag nanorod was used as an extra line defect inside the SWG, and the field enhancement is anticipated with the local mode of the surface plasmon polaritons (SPPs).

We clarify the merits for image transfer that we use the line defect (Ag nanorod in the SWG) to create an SWG for the application of image transfer in the nano-dimension. The SWG is illuminated normally by the incident beam with z-polarization from below. Once the incident beam is illuminated inside the SWG, it has nowhere else to go where one channel (Ag nanorod) is dropped at one carrier wavelength. The other parameters used are cell size $\Delta x=\Delta y=\Delta z=\Delta=1$ nm, and the total space volume considered consists of $101(x)\times 101(y)\times 101(z)$ cells. The time step is chosen to be $\Delta t=0.95/c(\Delta x^{-2}+\Delta y^{-2}+\Delta z^{-2})^{-1/2}$, where c is the speed of light. We iterate 5000 steps of the field calculations to achieve convergence. The incident Gaussian beams with full width at half-maximum (FWHM) were adjusted[22] such that FWHM$=0.5\lambda/$NA. The permittivity of Ag is set as $\epsilon=-9.121+i0.304$ at wavelength $\lambda=488$ nm,[17,18] and the numerical aperture (NA) of the objective lens is 0.85.

Figure 2 shows the field intensity along x (at $y=50\Delta$ sectional plane, shown in Fig. 1) in the plane of (a) $z=10$ (the bottom of the rod), (b) $z=35$ (the center of the rod), (c) $z=60$ (the top of the rod), (d) $z=70$ (imaging plane, at the plane 10 nm away from the rod), and (e) $z=90$ (at the plane 10 nm away from the rod), respectively. It can be observed in Fig. 2 that the field intensities along the x axis (at $y=50\ \Delta$ sectional plane) in the plane of (a), (b), and (c) are higher than those of (d) and (e) due to the collection of SPPs. This phenomenon can be explained. For an Ag nanorod whose size is much smaller than the incident wavelength, the optical responses are similar to dipoles, and the particle-particle interactions are similar to dipole-to-dipole interactions. When the size of a metallic rod is very small, for example, less than 100 nm, plasmons may play a role in the interaction of optical radiation with a nanorod. In the near-field zone, the smaller the metal rod is, the more the effects of the surface atoms of the nanorod can be seen. Indeed, according to the frequency-dependent metal properties, localized eigenmodes characterized by evanescent wave functions may be sustained by small objects and even by surfaces.

The atoms in the Ag nanorod along the circle edges of the top and bottom and the edge rims of the rod ends (top and bottom) can be considered as many dipoles at the symmetry positions around the circumference of the rod ends. The Ag nanorod we used here has an aperture opening of 20 nm at two ends of the rod. If we choose a rod diameter larger than 100 nm, the effect of the near-field is not more obvious than the smaller rod. The higher-order modes for longer rods can be also excited at the same frequency. The propagation length of SPP along a nanorod was theoretically investigated,[23] and an experimental result of SPP propagation along a nano-wire was also reported.[24,25] From the results of our simulations, we find that with the smaller-diameter (less than 100 nm) nanorod, a larger number of

Downloaded From: http://opticalengineering.spiedigitallibrary.org/ on 04/26/2014 Terms of Use: http://spiedl.org/terms

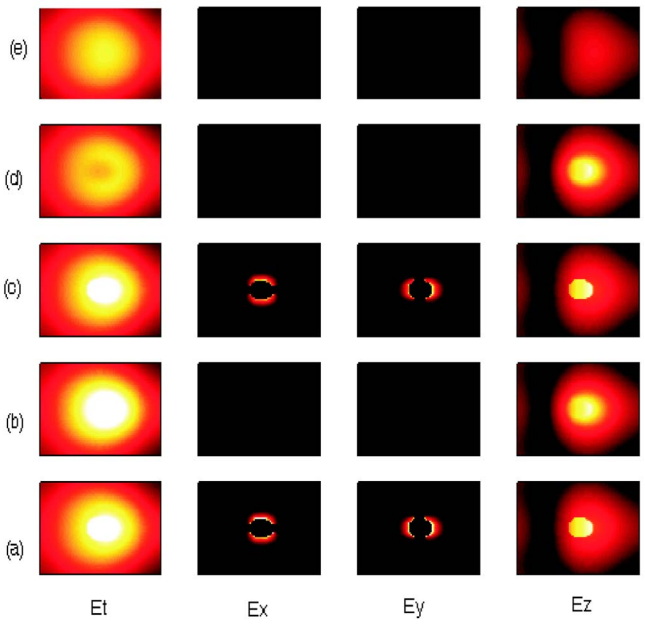

Fig. 3 Field propagation process in the image transfer obtained at each longitudinal position, i.e., (a) to (e) (*x-y* sectional plane at different *z* values, as shown in Fig. 1) by the 3D FDTD.

surface plasmons can be excited, which interact with the incident field and form the localized field enhancement. This is to be expected because many surface charge densities will be induced in the circumference of the two ends of the rod by the incident electric fields. The strongest field intensity (peak value) is found at the circumference of the top and bottom facet of the Ag nanorod [see (a) and (c) in Fig. 2]. Note that the localized electric field enhancement at the edge along the top and bottom extends in the tens of nanometers range from the rod top [see (d) in Fig. 2]. The field enhancement of the Ag nanorod originates mainly from the localized surface plasmon mode excited by the evanescent field. These near-field optical phenomena of the metallic nanostructure correspond to the near-field optical properties that were found in previous simulations[5] and experiments.[22]

In order to realize the detailed behaviors of the field distribution inside the nanorod, the three components of the field distribution will be discussed here. To find the contribution of SPPs, we plot the polarization components of the field. The polarized incident wave is enhanced in the Ag nanorod and decayed gradually after exiting the end of the rod, producing two perpendicularly polarized electric field components—that is, the incident field is entirely polarized along the z axis and the scattered field also has components along the x axis and y axis, respectively. These components produce depolarization at this interface between the top of rod and the dielectric background. A more-detailed calculation using the 3D FDTD method is shown in Fig. 3, which illustrates the beam profile in the image transfer obtained at each longitudinal position ($x-y$ sectional plane at different z positions). Figure 3 shows the distributions of the total electric field and field components in the plane away from the object plane along (a) $z=10$, (b) $z=35$, (c) $z=60$, (d) $z=70$, and (e) $z=90$, respectively (from bottom to top). From left to right, Fig. 3 shows $|E_t|$ (the total intensity distribution), $|E_x|$, $|E_y|$, and $|E_z|$. The size of each image plane displayed is 100×100 nm^2. The x and y components of the electric field are distributed symmetrically along the rim of the bottom [Fig. 3(a)] and top [Fig. 3(c)] of the rod, showing two petal distributions much smaller than that of the z component. As discussed earlier, an interesting enhancement occurs at the circumference of the rod ends. Both $|E_x|$ and $|E_y|$ decay rapidly as the distance from the rod increases. The z component of the electric field leads to propagation mainly in the forward direction along the probe axis. This component is the same as that of the polarization direction of the incident field. The depolarization phenomenon of components is the near-field effect. Note that the components of E_x and E_y are not found at the middle plane of the rod [Fig. 3(b)].

Figures 3(a)–3(e) gives us the mechanism of the image transfer shown in Fig. 1. A z polarized Gaussian beam near the entrance surface of a nanorod excites a longitudinal electron oscillation along the rod. It can be seen in Fig. 3(d) that the intensity distribution at the plane 10 nm away from the rod shows that the FWHM of the light spot is nearly 40 nm, and the light is well resolved. This oscillation corresponds to the fundamental mode of the SPP resonance. The oscillating $|E_z|^2$ field is enhanced at the rod end to provide the intensity of the subwavelength image. The spot diameter is as small as that of the rod. Figure 3(e) shows the intensity distribution at $z=90$ nm, or 30 nm from the rod. The spots are somewhat blurred, while the light spot is still clearly resolved. This result shows that the nanopattern can be image-transferred through an Ag nanorod or rod array containing the subwavelength resolution. The spatial resolution is 40 nm, which is far above the diffraction limit.

In conclusion, we have presented the numerical results for calculating the near-field distributions of a silver nanorod by using the 3D FDTD method and confirmed that the silver nanorod is a useful device for super-resolution near-field imaging. The resolution in our case used parameters higher than those of conventional diffraction-limited optics with spatial resolution exceeding the wavelength of the incident illumination. Our device enables a deep transfer of the image without loss and can be used for image transfer. The high intensity of the optical field at the output end emerging from the nanorod may give rise to physically observable phenomena in the near-field zone. These properties arising from the field at the output end of the nanorod can be associated with the enhanced spatial resolution in photolithography, used to promote the data storage capability in optical memory systems, used as functional building blocks for nanoscale wave-guiding devices and sensors and optoelectronics, as well as other applications.

Acknowledgments

This project is financially sponsored by the National Science Council (Grant No. NSC 95-2112-M-231-001) and the Ministry of Economics (Grant No. 95-EC-17-A-08-S1-0006).

References

1. V. M. Shalaev, *Optical Properties of Nanostructured Random Media*, Springer, Berlin (2002).

Downloaded From: http://opticalengineering.spiedigitallibrary.org/ on 04/26/2014 Terms of Use: http://spiedl.org/terms

2. S. Kawata, *Near-field and Surface Plasmon Polaritons*, Springer, Berlin (2001).
3. J. R. Krenn, "Nanoparticle waveguides watching energy transfer," *Nat. Mater.* **2**, 210–211 (2003).
4. M. L. Brongersma, J. W. Hartman, and H. A. Atwater, "Electromagnetic energy transfer and switching in nanoparticle chain arrays below the diffraction limit," *Phys. Rev. B* **62**(24), R16356 (2000).
5. Y. F. Chau, T. J. Yang, and D. P. Tsai, "Imaging properties of three dimensional aperture near-field scanning optical microscopy and optimized near-field fiber probe designs," *Jpn. J. Appl. Phys.* **43**, 8115–8125 (2004).
6. Y. F. Chau, T. J. Yang, and D. P. Tsai, "Near-field optics simulation of a solid immersion lens combining with a conical probe and a highly efficient solid immersion lens-probe system," *J. Appl. Phys.* **95**(7), 3378–3384 (2004).
7. S. A. Maier, P. G. Kik, and H. A. Atwater, "Optical pulse propagation in metal nanoparticle chain waveguides," *Phys. Rev. B* **67**, 205402 (2003).
8. N. Hayazawa, Y. Inouye, Z. Sekkat, and S. Kawata, "Near-field Raman scattering enhanced by a metallized tip," *Chem. Phys. Lett.* **335**, 369–374 (2001).
9. T. Ichimura, N. Hayazawa, M. Hashimoto, Y. Inouye, and S. Kawata, "Tip-enhanced coherent anti-Stokes Raman scattering for vibrational nanoimaging," *Phys. Rev. Lett.* **92**(22), 220801 (2004).
10. E. Prodan, C. Radloff, N. J. Halas, and P. Nordlander, "A hybridization model for the plasmon response of complex nanostructures," *Science* **302**(17), 419–422 (2003).
11. T. W. Ebbesen, H. J. Lezec, H. F. Ghaemi, T. Thio, and P. A. Wolff, "Extraordinary optical transmission through sub-wavelength hole arrays," *Nature (London)* **391**(12), 667–669 (1998).
12. H. J. Lezec, A. Degiron, E. Devaux, R. A. Linke, L. M. Moreno, F. J. G. Vidal, and T. W. Ebbesen, "Beaming light from a subwavelength aperture," *Science* **297**, 820–822 (2002).
13. N. R. Jana, L. Gearheart, and C. J. Murphy, "Wet chemical synthesis of high aspect ratio cylindrical gold nanorods," *J. Phys. Chem. B* **105**, 4065–4067 (2001).
14. W. L. Barnes, A. Dereux, and T. W. Ebbesen, "Surface plasmon subwavelength optics," *Nature (London)* **424**(14), 824–830 (2003).
15. J. B. Pendry, "Negative refraction makes a perfect lens," *Phys. Rev. Lett.* **85**(18), 3966–3969 (2000).
16. X. S. Rao and C. K. Ong, "Subwavelength imaging by a left-handed material superlens," *Phys. Rev. E* **68**, 067601 (2003).
17. A. Ono, J. Kato, and S. Kawata, "Subwavelength optical imaging through a metallic nanorod array," *Phys. Rev. Lett.* **95**, 267407 (2005).
18. A. Taflove, *Computational Electrodynamics: The Finite-Difference Time-Domain Method*, 2nd ed., Artech House, Norwood, MA, (2000).
19. J. P. Berenger, "A perfectly matched layer for the absorbing boundary condition," *J. Chem. Phys.* **114**, 185–200 (1994).
20. J. B. Judkins and R. W. Ziolkowski, "Finite-difference time-domain modeling of nonperfectly conducting metallic thin-film gratings," *J. Opt. Soc. Am. A* **12**(9), 1974–1983 (1995).
21. K. S. Kunz and R. J. Lubbers, *The Finite Difference Time Domain Method for Electromagnetics*, CRC Press, Boca Raton, FL (1993).
22. T. Nakano, A. Sato, H. Fuji, J. Tominaga, and N. Atoda, "Transmitted signal detection of optical disks with a superresolution near-field structure," *Appl. Phys. Lett.* **75**(2), 151–153 (1999).
23. J. Takahara, S. Yamagishi, H. Taki, A. Morimoto, and T. Kobayashi, "Guiding of a one-dimensional optical beam with nanometer diameter," *Opt. Lett.* **22**(7), 475–477 (1997).
24. R. M. Dickson and L. A. Lyon, "Unidirectional plasmon propagation in metallic nanowires," *J. Phys. Chem. B* **104**, 6095–6098 (2000).
25. J. C. Weber, A. Dereux, C. Girard, J. R. Krenn, and J. P. Goudonnet, "Plasmon polaritons of metallic nanowires for controlling submicron propagation of light," *Phys. Rev. B* **60**(12), 9061–9068 (1999).

Downloaded From: http://opticalengineering.spiedigitallibrary.org/ on 04/26/2014 Terms of Use: http://spiedl.org/terms